# LARGE EDDY SIMULATIONS OF TURBULENT MIXED CONVECTION IN A VERTICAL PLANE CHANNEL

**S. K. Yan, C. Y. Wang**
Institute of Aeronautics and Astronautics,
National Cheng Kung University
Tainan, Taiwan, R.O.C
qfwfq612@yahoo.com.tw, chenwang@mail.ncku.edu.tw

## ABSTRACT

A series of large eddy simulations of fully developed turbulent mixed convection for adding flow condition in a vertical plane channel are performed. The Reynolds number is $Re_b = 5600$ (based on the bulk velocity and the channel width), the Prandtl number is 0.71. Several different Grashof numbers are computed to cover a wide range of flow phenomena.

The first order, second order statistics and instantaneous streamwise velocity and temperature fluctuation fields in the Near-wall Region are examined to study the influence of buoyancy on turbulent structures.

## INTRODUCTION

Turbulent mixed convection in vertical tubes or channels receives considerable attention because of wide applications in engineering. In the past sixty years, the turbulent mixed convection in vertical channels and tubes have been studied extensively through experimental or theoretical methods. The recent reviews are given by Jackson et al. (1989) and Petukhov and Polyakov (1988). The influence of buoyancy depends on the directions of two driving forces, mean pressure gradient and buoyancy, and we only consider the aiding flow condition in this paper. In aiding flow, upward heated flow or downward cooled flow, the heat transfer rate decreases first and then increases again with increasing the strength of buoyancy.

In contrast to the heat transfer rate, only few papers studied the modification of turbulent structures under the action of buoyancy. Carr et al. (1973) and Polyakov and Shindin (1988) studied experimentally the upward air flow in a heated vertical tube to examine the influence of buoyancy on turbulent structures. Kasagi and Nishmura (1997) performed a series of direct numerical simulations to study the effect of buoyancy in a differentially heated vertical plate channel, where the aiding flow condition occurs near the heated wall.

In this paper, a series of large eddy simulations of fully developed turbulent mixed convection for aiding flow condition in a vertical plane channel are performed to study the effects of buoyancy.

## NUMERICAL METHOD

The computational domain for LES of turbulent mixed convection in a vertical channel is shown in Fig. 1 The $x$, $y$, and $z$ directions denote the streamwise, wall-normal, and spanwise directions, respectively.

The governing equations are the filtered versions of the incompressible Navier-Stokes equations with the Boussinesq approximation, the continuity equation, and the energy equation. Periodic boundary conditions are are used in the streamwise and spanwise directions, and the non-slip boundary condition and constant heat flux are imposed on the walls. The Langrangian versions of the dynamic eddy viscosity and diffusivity models (Meneveau,1996) are used to model the Sub-grid Scale (SGS) stress and heat flux.

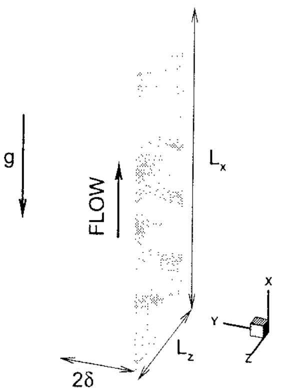


Figure 1: Computational domain for LES

A modified fourth order accurate scheme of Morinishi et al. (1998) on a staggered grid system (Yan, 2002) which simultaneously conserves mass, momentum ,and kinetic energy on a non-uniform grid system is employed for the spatial terms. The governing equations are integrated in time using a hybrid three-step Runge-Kutta/Crank-Nicholson time advance method (Spalart,1991). The implicit Crank-Nicholson scheme is used for the diffusion terms in the wall normal direction and a third order explicit Runge-Kutta method is used for all other terms. The fractional step method of Dukowicz and Dvinsky (1992) is used to enforce the divergence-free condition at every sub-step. A FFT(fast Fourier transform)-based direct solution is used to solve the discrete Poission equation for pressure.

The Reynolds number is $Re_b = 5600$ (based on the bulk velocity $U_b$ and the channel width $2\delta$) and the Prandtl number is 0.71. Several different Grashof numbers, based on the wall heat flux and the hydraulic diameter, are computed to cover a wide range of flow phenomena and are summarized in Table 1.

It is inadequate to use a single computational configuration for all cases since turbulent structures change significantly under the influence of buoyancy. The grid sizes, $96 \times 65 \times 96$ in the streamwise, wall-normal, and spanwise

Table 1: Cases for aiding flow

| Case | $Gr_q$ | $L_x$ | $L_z$ | $\Delta t$ |
|---|---|---|---|---|
| a50 | $1.06 \times 10^8$ | $4.0\pi\delta$ | $1.5\pi\delta$ | $0.05U_b/\delta$ |
| a125 | $1.40 \times 10^8$ | $9.0\pi\delta$ | $4.0\pi\delta$ | $0.15U_b/\delta$ |
| a250 | $3.55 \times 10^8$ | $6.0\pi\delta$ | $3.0\pi\delta$ | $0.125U_b/\delta$ |
| a500 | $5.28 \times 10^8$ | $4.0\pi\delta$ | $1.5\pi\delta$ | $0.05U_b/\delta$ |
| a1000 | $2.53 \times 10^9$ | $3.5\pi\delta$ | $1.3\pi\delta$ | $0.05U_b/\delta$ |

Table 2: Nusselt numbers and friction coefficients

| Case | $Gr_q$ | $Nu$ | $C_f$ |
|---|---|---|---|
| a50 | $1.06 \times 10^8$ | 31.56 | $7.74 \times 10^{-3}$ |
| a125 | $1.40 \times 10^8$ | 16.34 | $6.81 \times 10^{-3}$ |
| a250 | $3.55 \times 10^8$ | 21.18 | $9.37 \times 10^{-3}$ |
| a500 | $5.28 \times 10^8$ | 28.12 | $1.31 \times 10^{-2}$ |
| a1000 | $2.53 \times 10^9$ | 38.59 | $1.83 \times 10^{-2}$ |

directions, respectively, are the same for all cases, while the computational lengths in the streamwise and spanwise directions change according to the streamwise and spanwise two-point correlations, which should decay to a sufficient low value at half the length of the maximum separation to include the largest scale eddies in the flow and reduce the influences of artificial periodic boundaries on turbulent statistics to a minimum. The computational lengths in streamwise and spanwise directions are listed in Table 1. The grid spacings are uniform in periodic directions, and the grid points are clustered according to a hyperbolic tangent function in the normal direction.

The initial flow and temperature fields are obtained from a coarse grid LES. The time steps are summarized in Table 1. Most cases use $\Delta t = 0.05U_b/\delta$ and time steps increase at the intermediate Grashof numbers. For each case, the computation is run for 2500 time steps to reach the statistically steady state, and then the statistics are sampled by averaging the homogeneous directions at every two time-step over 7500 – 10000 steps.

The grid independence tests are performed at three representative Grashof numbers with grid resolutions ranging from $64 \times 65 \times 64$ to $112 \times 81 \times 112$. The first order statistics are nearly indiscernible for the finer grid resolutions, and the second order statistics show larger discrepancies on some cases due to sub-grid scale motions under-resolved at the low grid resolutions or insufficient samples at the finest grid resolution.

## TURBULENT STATISTICS

### Nusselt Number

The friction coefficients, $C_f = 2\tau_w/\rho U_b^2$, and the Nusselt numbers, $Nu = 4h\delta/\kappa$, for different Grashof numbers are listed in Table 2. $Nu$ shows a drastic reduction, only 45% of that at $Gr_q = 0$, around $Gr_q = 1.40 \times 10^8$. This implies the self-sustaining mechanisms of wall turbulence are destroyed largely by buoyancy. Then the Nusselt number grows again because the intensity of turbulence generated by buoyancy increases as $Gr_q$ is increased. The friction coefficient shows a similar but less drastic reduction, 85% of the friction coefficient at $Gr_q = 0$. As $Gr$ is increased, the friction coefficient first decreases because of the reduction of the intensity of turbulence and then grows very fast because of an increase of the mean streamwise velocity in the near-wall region.

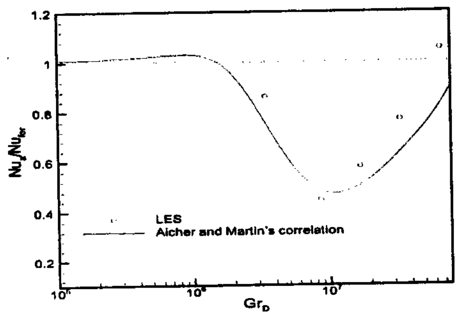


**Figure 2: Nusselt numbers**

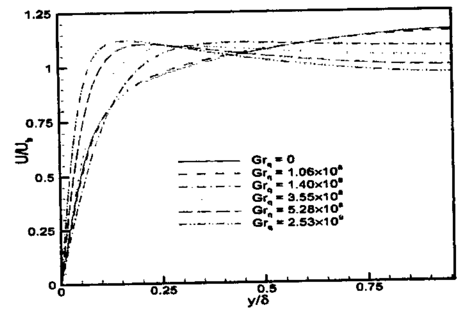


**Figure 3: Mean streamwise velocities normalized by $U_b$**

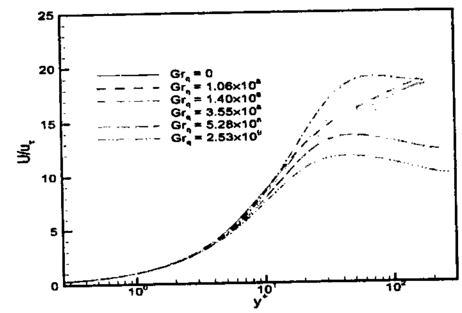


Figure 4: Mean streamwise velocities normalized by $u_\tau$

A comparison of $Nu$ for adding flow with the Aicher and Martin's empirical correlation (Aicher and Martin, 1997) is presented in Figure 2. $Gr_D$ represents the Grashof number based on the temperature difference between the bulk temperature and wall temperature and the hydraulic diameter. Although some discrepancy is observed, the tendency from LES is similar to that from the empirical correlation. The present Nusselt numbers show a better agreement with the Aicher and Martin's correlation in the decay region than in the recovery region.

### Mean Streamwise Velocity and Temperature

The mean streamwise velocity profiles normalized by the

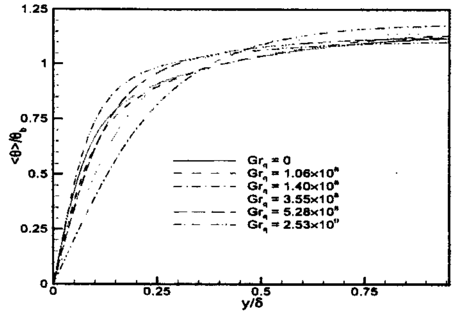


**Figure 5: Mean temperatures normalized by $\theta_b$**

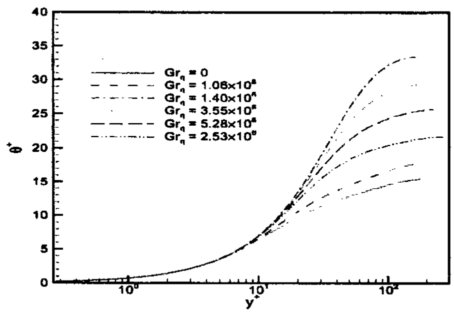


Figure 6: Mean temperatures normalized by $\theta_\tau$

mean bulk velocity, $U_b$, for aiding flow are displayed in Figures 3. For aiding flow, $Gr_q = 1.40 \times 10^8$ can be viewed as a transition point. Before the transition $Gr_q$, the mean velocity decreases in the central region and near-wall region and the resulting velocity slope in the near-wall region also decreases with increasing $Gr_q$. At the transition $Gr_q$, $Gr_q = 1.40 \times 10^8$, the velocity maximum point moves away from center and the velocity slope in the near wall region declines to a minimum. After the transition $Gr_q$, the mean velocity decreases and increases in the central region and near-wall region, respectively, with increasing $Gr_q$. The maximum value of the mean velocity profile increases and its location moves toward the wall with increasing $Gr_q$. The asymptotic profile with increasing $Gr_q$, observed by Carr et al. (1973) at a similar Reynolds number, doesn't appear.

The mean streamwise velocity profiles in wall coordinates, normalized by the friction velocity, $u_\tau$, for aiding flow are showed in Figure 4. After the transition $Gr_q$, the logarithmic region disappears and the maximum value reduces significantly because the wall shear stress increases very fast with an increase of $Gr_q$.

Figure 5 shows the mean temperature profiles normalized by the mean bulk temperature, $\theta_b$, for aiding flow. Before the transition $Gr_q$, the temperature profile increases and decreases slightly in the central region and near-wall region, respectively. Because the turbulence is suppressed by buoyancy at $Gr_q = 1.40 \times 10^8$, the slope at the wall decreases to a minimum, corresponding to a minimum Nusselt number, and the value at the center reaches a maximum. After the transition $Gr_q$, the slope in the near-wall region increases again and the temperature in the central region decreases with an increase of $Gr_q$ . Figure 6 shows the mean temperature profiles in wall coordinates, normalized by the friction temperature, $\theta_\tau$, for aiding flow. The profile collapses in

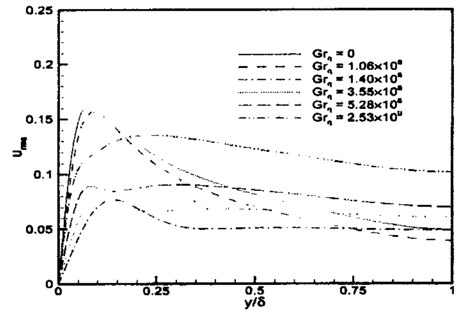


**Figure 7: Streamwise velocity fluctuations normalized by $U_b$**

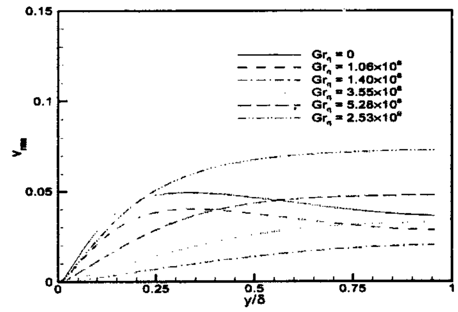


**Figure 8: wall-normal velocity fluctuations normalized by $U_b$**

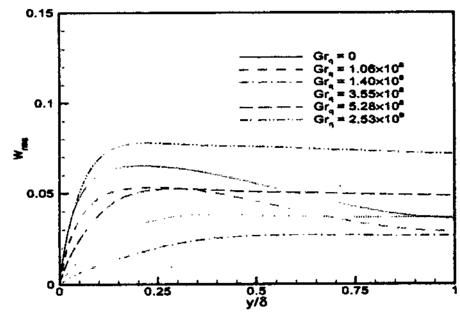


Figure 9: Spanwise velocity fluctuations normalized by $U_b$

the sublayer region, $y^+ < 5$, and follow the linear law of the wall very well. The profile first shifts upward and reaches the highest value at $Gr = 1.40 \times 10^8$ due to a decrease of the friction temperature. After the transition $Gr_q$, the profile shifts downward due to the increase of the friction temperature.

### Turbulence Intensities

Figure 7 to 9 show the streamwise, wall-normal and spanwise velocity intensities, respectively, normalized by $U_b$, in aiding flow. There are two distinct types of velocity fluctuations. When $Gr_q$ is smaller than the transition $Gr$, the main ingredient of velocity fluctuations induces from the shear stress. So the velocity intensities decrease gradually with an increase of $Gr_q$. Kasagi and Nishmura (1997) performed DNS for a similar type flow at low $Gr$ and showed a similar trend in the near wall region. As $Gr_q$ is increased

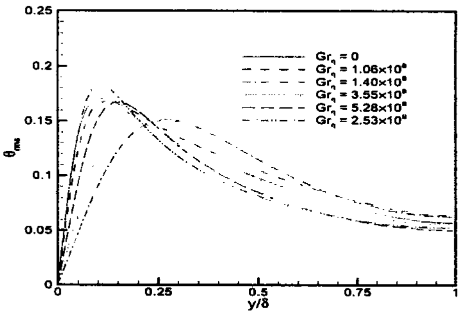


Figure 10: Temperature fluctuations normalized by $\theta_b$

slightly from $1.06\times10^8$ to $1.40\times10^8$, the intensities suddenly deteriorate significantly in most regions except in the central region where $u_{rms}$ even increases and the most severest decay occurs in the near-wall region. This is because the self-sustaining mechanisms of turbulence in the near-wall region are destroyed largely by buoyancy. The maximum values of $v_{rms}$ and $w_{rms}$ shift to the center and $y \approx 0.6$, respectively, from the near-wall region, and the profiles of $u_{rms}$ and $w_{rms}$ show flat distributions when $y > 0.35$ and $y > 0.5$, respectively.

After the transition $Gr_q$, the turbulence generated by buoyancy increases its influence on the velocity fluctuations. The profiles of $v_{rms}$, $w_{rms}$ and $u_{rms}$ away from the wall are similar to those of natural convection between two infinite vertical differentially heated walls (Versteegh and Nieuwstadt, 1999). In addition to the local maximum (first maximum) generated by the shear force, $u_{rms}$ shows another local maximum (second maximum) away from the wall. Both local maximums grow and move toward the wall with increasing $Gr_q$ and the growth rate of the second maximum exceeds that the first maximum's. The value of the second maximum exceeds that of the first maximum at $Gr_q = 5.28\times10^8$, and at $Gr_q = 2.53\times10^9$ the first maximum disappears. This indicates the turbulence generated by buoyancy becomes a dominant ingredient. All profiles of $v_{rms}$ have a similar shape, a local maximum at channel center, while the magnitude increases with increasing $Gr_q$. The local maximum of $w_{rms}$ shifts toward the wall with increasing $Gr_q$. The profiles are nearly flat from the local maximum point to the center, although a slow decay is observed. While comparing with Carr et al. (1973) and a similar trend for $u^+_{rms}$ is found.

### Temperature Fluctuation

Figure 10 shows the rms of temperature fluctuation, $\theta_{rms}$, normalized by $\theta_b$ in aiding flow. Before the transition $Gr_q$, the temperature fluctuation increases in most regions except for $y < 0.1$. At $Gr_q = 1.40\times10^8$, the temperature fluctuation decays severely in $y < 0.25$ and grows in the other regions. After the transition $Gr_q$, the temperature variance grows in the near-wall region and the maximum value increases and shifts toward the wall with an increase of $Gr_q$ . While comparing with Carr et al. (1973), the trend for $\theta_{rms}$ is rather different. Experiment errors are a possible reason for the discrepancy.

### Reynolds Shear Stress

Figure 11 shows the Reynolds shear stress, $-\langle u''v''\rangle - \langle\tau_{12}\rangle$, normalized by $U_b^2$ in aiding flow. Before the transition $Gr_q$, the Reynolds shear stress decreases as $Gr_q$ is increased and the profile is similar to that at $Gr_q = 0$. At $Gr = 1.40\times10^8$, the Reynolds shear stress suddenly declines to a very low level, which the maximum value is only 8% of that at $Gr_q = 0$, because the self-sustaining mechanisms of wall turbulence are destroyed largely by buoyancy. The Reynolds shear stress changes sign at nearly same location of the maximum velocity, where the shear production term in the budget of $\langle u''v''\rangle$, $-\langle v''^2\rangle\partial U/\partial y$, also changes sign. When $Gr_q$ is increased further, the portion of negative Reynolds shear stress increases and the positive Reynolds shear stress only exists in the near-wall region. The absolute values of the extreme values of Reynolds shear stress increases and shifts toward the wall. The absolute value of the maximum value of the Reynolds shear stress is 3.6 times larger than the positive Reynolds shear stress at $Gr = 2.53\times10^9$. The similar trends are found by Carr et al. (1973) and Polyakov and Shindin (1988) while their values have some deviations.

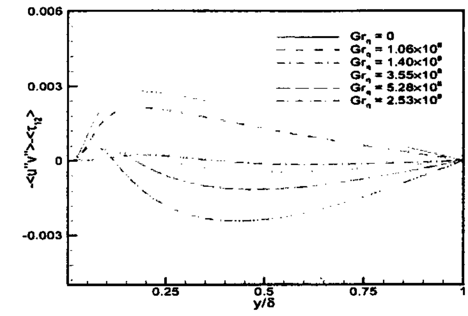


**Figure 11: Reynolds shear stress normalized by $U_b^2$**

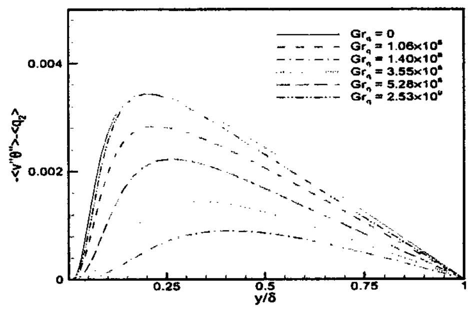


Figure 12: Wall-normal turbulent heat flux normalized by $U_b\theta_b$

### Turbulent heat flux

Figure 12 shows the wall-normal turbulent heat flux, $-\langle v''\theta''\rangle - \langle q_2\rangle$, normalized by $U_b\theta_b$ in aiding flow. Before the transition $Gr_q$, the wall-normal turbulent heat flux drops gradually with an increase of $Gr_q$ . At $Gr_q = 1.40\times10^8$, the wall-normal turbulent heat flux shows a less severe decay than the Reynolds shear stress away from the wall since temperature becomes active. The maximum value is about 26% of that for $Gr_q = 0$ and shifts from $y = 0.2$ to $y = 0.4$. After the transition $Gr_q$, the wall-normal turbulent heat flux grows as $Gr_q$ is increased and the maximum point shifts to the wall. The profiles after the transition are similar to those

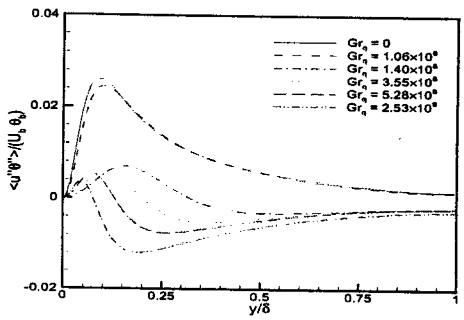


**Figure 13: Streamwise turbulent heat flux normalized by $U_b\theta_b$**

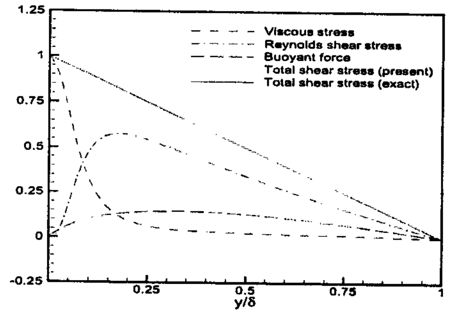


Figure 14: Shear stress balance at $Gr_q = 1.06 \times 10^8$

before the transition. At $Gr_q = 2.53 \times 10^9$, the profile is similar to that at $Gr_q = 0$ and the Nusselt numbers of both are nearly the same.

Figure 13 shows the streamwise turbulent heat flux, $\langle u''\theta''\rangle$, normalized by $U_b\theta_b$ in aiding flow. There are two distinct types of profile, similar to the Reynolds shear stress, due to the direct influence of buoyancy to the streamwise velocity. Before the transition $Gr_q$, the streamwise turbulent heat flux decreases slightly for $y < 0.13$. At $Gr_q = 1.40 \times 10^8$, the streamwise turbulent heat flux decay significantly and changes sigh for $y > 0.36$ which is slighter before the location of the maximum streamwise velocity ($y \simeq 0.4$). After the transition $Gr_q$, the portion of $\langle u''\theta''\rangle < 0$ increases with increasing $Gr_q$ because the location of the maximum streamwise velocity shifts to the wall. With an increase of $Gr_q$, the absolute value of the maximum values on the side of $\langle u''\theta''\rangle < 0$ and $\langle u''\theta''\rangle > 0$ increases and decreases, respectively, while the maximum points on both sides shift toward the wall.

### Shear Stress Balance Equation

By integrating the mean streamwise momentum equation from the wall to $y$, the shear stress balance equation is obtained

$$\frac{1}{Re_\tau}\frac{d\langle u^+\rangle}{dy} - \langle u''^+ v''^+\rangle - \langle \tau_{12}^+\rangle - \frac{Gr}{Re_\tau}\int_0^y (\langle\theta\rangle - \theta_{ar})dy = 1 - y \qquad (1)$$

where $\theta_{ar}$ is the arithmetic mean temperature. The four terms on the left-hands side of Eq. 1 are the viscous stress, the resolved Reynolds shear stress, the SGS shear stress

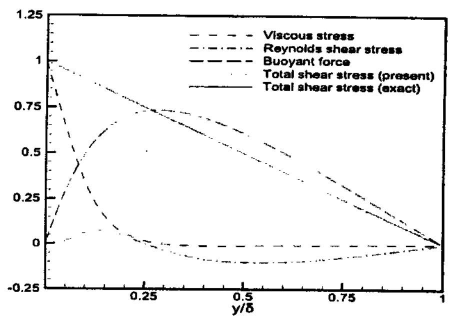


Figure 15: Shear stress balance at $Gr_q = 3.55 \times 10^8$

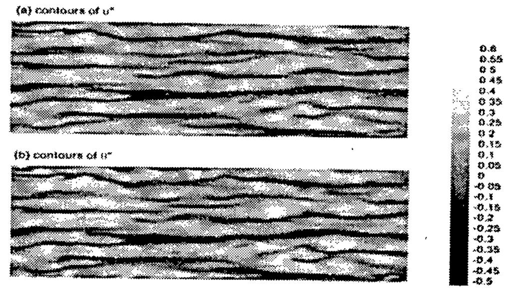

Figure 16: Contours of $u''$ and $\theta''$ at $Gr_q = 1.06 \times 10^8$

and the buoyant force, respectively, and the Reynolds shear stress is the sum of the resolved Reynolds shear stress and the SGS shear stress. The sum of these four terms equals to the mean pressure gradient, which is the right-hand side of Eq. 1.

Figures 14 and 15 show the budget terms for the shear stress balance at $Gr_q = 1.06 \times 10^8$ and $Gr_q = 3.55 \times 10^8$, respectively, in aiding flow. In aiding flow, the contribution of the buoyant force is the same direction as that of the Reynolds shear stress, so an increase of the buoyant force will decrease the strength of the Reynolds shear stress. The contribution of the Reynolds shear stress to the total shear stress is much larger than the buoyant force at $Gr_q = 1.06 \times 10^8$, while the role changes with a slight increase of $Gr_q$ to $1.40 \times 10^8$, which the Reynolds shear stress suddenly reduces to a very low level. This implies there exists a threshold and the self-sustaining mechanism of wall turbulence will be destroyed largely when $Gr_q$ exceeds the threshold. The Reynolds shear stress becomes negative in the central region due to buoyancy and the buoyant force exceeds the total shear stress in the same region. The domain of $-\langle u''v''\rangle - \langle\tau_{12}\rangle < 0$ becomes larger with an increase of $Gr_q$ .

### Instantaneous Fields in The Near-wall Region

Figures 16 to 18 show the contours of the instantaneous streamwise velocity (normalized by $U_b$) and temperature (normalized by $\theta_b$) fluctuations at $y \approx 0.05$ at three different $Gr_q$ s in aiding flow.

At $Gr_q = 1.06 \times 10^8$ the structure is very similar to that at $Gr_q = 0$. The well-known alternating low- and high-speed streaky structures, responsible for most of production of turbulent energy and momentum and energy transfer, are observed, while those structures are less distorted and more

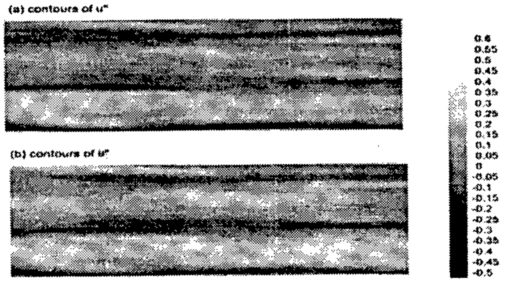


Figure 17: Contours of $u''$ and$\theta''$ at $Gr = 1.40 \times 10^8$

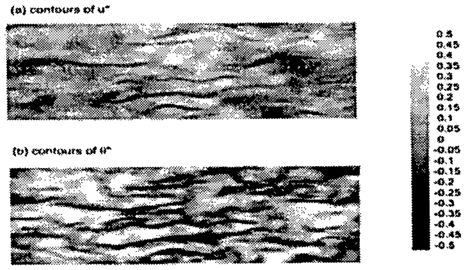


Figure 18: Contours of $u''$ and $\theta''$ at $Gr_q = 2.53 \times 10^9$

elongated and stable than those at $Gr_q = 0$. Fig. 16 indicate that $\theta''$ is highly correlated with $u''$, thus the low-speed fluid is associated with the low-temperature fluid and the high-speed fluid is associated with the the high-temperature fluid. Note the higher $\theta$ indicate the lower true temperature.

At $Gr_q = 1.40 \times 10^8$ (Figure 17), the action of buoyancy is strong enough to destroy most of regeneration processes of the low- and high-speed streaks. Only weak and inactive streaks exist. The mean length of the low-speed streaks is at least twice as long as those at $Gr_q = 0$.

At the highest simulated $Gr_q = 2.53 \times 10^9$, Figure 18 shows the streaky structures nearly disappear, as evidenced by the disappearance of the negative local minimum for the spanwise two-point correlation functions for $u''$ and $\theta''$. The similarity between $u''$ and $\theta''$ greatly deteriorates and the cross correlation coefficient between $u''$ and $\theta''$ is only about 0.4 in the near wall region. The regions with large temperature fluctuations occur locally like distorted patches. This indicates the thermal plumes gradually become the dominate turbulent structures.

## CONCLUSIONS

A transition Grashof number exists in aiding flow at the calculated Reynolds number and Prandtl number.

Before the transition $Gr_q$, the turbulence is generated mostly by the shear force driven by the pressure gradient and the turbulence intensity decreases with increasing the buoyant force. Around the transition $Gr_q$, the generation process of near-wall structures are destroyed mostly, thus the velocity fluctuations and temperature fluctuation in the near-wall region show the severest deterioration and the friction coefficient and Nusselt number decline to 85% and 45%, respectively, of that at $Gr_q = 0$. After the transition $Gr_q$, turbulence generated by buoyancy gradually becomes a dominant ingredient.

## REFERENCES


Aicher, T., and Martin, H., 1997,"New Correlations for Mixed Turbulent Natural and Forced Convection Heat Transfer in Vertical Tubes," *Int. J. Heat Mass Transfer*, Vol. 40, pp. 3617-3626.

Carr, A. D., Connor, M. A., and Buhr, H. O., 1973, "Velocity, Temperature, and Turbulence Measurements in Air for Pipe Flow with Combined Free and Forced Convection," *ASME J. Heat Transfer*, Vol. 95, pp. 445-452.

Dukowicz, J. K., and Dvinsky, A. S., "Approximation as a Higher Order Splitting for the Implicit Incompressible Flow Equations," *J. Comput. Phys.*, Vol. 102, 1992, pp. 336-347.

Jackson, J. D., Cotton, M. A., and Axcell, B. P., 1989, "Studies of Mixed Convection in Vertical Tubes," *Int. J. Heat Fluid Flow*, Vol. 10, pp. 2-15.

Jackson, J. D., and Fewster, J., 1977,"Enhancement of Heat Transfer due to Buoyancy for Downward Flow of Water in Vertical Tube," *Heat Transfer and Turbulent Buoyant Convection*, edited by D. B. Spalding and N. Afgan, Hemisphere, Washington D. C., pp. 759-775.

Kasagi, N., and Nishimura, M., 1997,"Direct Numerical Simulation of Combined Forced and Natural Turbulent Convection in a Vertical Plane Channel," *Int. J. Heat Fluid Flow*, Vol. 18, pp. 88-99.

Meneveau, C., Lund, T. S., and Cabot, W. H., 1996, "A Lagrangian Dynamic Subgrid-Scale Model of Turbulence," *J. Fluid Mech.*, Vol. 319, pp. 353-385.

Morinishi, Y., Lund, T. S., Vasilyev, O. V., and Moin, P., 1998, "Fully Conservative Higher Order Finite Difference Schemes for Incompressible Flow," *J. Comput. Phys.*, Vol. 143, pp. 90-124.

Petukhov, B. S., and Polyakov, A. F., 1988, "*Heat Transfer in Turbulent Mixed Convection*," edited by B. E Launder, Hemisphere, Bristol, PA, USA, chapter 5.

Polyakov, A. F., and Shindin, S. A., 1988, "Development of Turbulent Heat Transfer over the Length of Vertical Tubes in the Presence of Mixed Air Convection," *Int. J. Heat Mass Transfer*, Vol. 31, pp. 987-992.

Spalart, P., Moser, R., and Rogers, M., 1991, "Spectral Methods for the Navier-Stokes Equations with on Infinite and Two Periodic Direction," *J. Comput. Phys.*, Vol. 96, pp. 297-324.

Swanson, L. W., and Catton, I.,1987, "Surface Renewal Theory for Turbulent Mixed Convection in Vertical Ducts," *Int. J. Heat Mass Transfer*, Vol. 30, pp. 2271-2279.

Versteegh, T. A. M., and Nieuwstadt, F. T. M., 1999,"A Direct Numerical Simulation of Natural Convection between Two Infinite Vertical Differentially Heated Walls Scaling Laws and Wall Functions," *Int. J. Heat Mass Transfer*, Vol. 42, pp. 3673-3693.

Yan, S. K., 2002, "Large Eddy Simulations of Turbulent Mixed Convection in a Vertical Plane Channel Using a New Fully-Conservative Scheme", Ph.D. Thesis, National Cheng Kung University, Tainan, Taiwan, R.O.C.